Vol. 8, No. 1, February 2024, pp. 80-85

Current Optics and Photonics

Regular Paper

Deep Learning-based Extraction of Auger and FCA Coefficients in 850 nm GaAs/AlGaAs Laser Diodes

Jung-Tack Yang, Hyewon Han, and Woo-Young Choi*

Department of Electrical and Electronic Engineering, Yonsei University, Seoul 03722, Korea

(Received October 30, 2023 : revised January 18, 2024 : accepted January 18, 2024)

Numerical values of the Auger coefficient and the free carrier absorption (FCA) coefficient are extracted by applying deep neural networks (DNNs) to the L-I characteristics of 850 nm GaAs/AlGaAs laser diodes. Two elemental DNNs are used to extract each coefficient sequentially. The fidelity of the extracted values is established through meticulous correlation of L-I characteristics bridging the realms of simulations and measurements. The methodology presented in this paper offers a way to accurately extract the Auger and FCA coefficients, which were traditionally treated as fitting parameters. It is anticipated that this approach will be applicable to other types of opto-electronic devices as well.

Keywords : Auger coefficient, Deep neural networks (DNN), FCA coefficient, Laser diode, L-I characteristic

OCIS codes : (100.4997) Pattern recognition, nonlinear spatial filters; (140.0140) Lasers and laser optics; (140.2020) Diode lasers; (140.3480) Lasers, diode-pumped; (140.5960) Semiconductor lasers

I. INTRODUCTION

The demand for laser diodes (LDs) continues to surge, owing to their inherent advantages, including compact size, cost-effectiveness, and exceptional power conversion efficiency [1–3] in various applications such as medical instruments [4, 5] and communication systems [6, 7]. Notably, they are investigated as crucial elements for sensing applications such as LiDAR [8–10] and facial expression or recognition systems [11, 12]. As their significance grows, there is a need to optimize their performance in the device design stage with simulation. Therefore, determining numerical values for key design parameters is essential for this. However, determining these experimentally presents challenges because measurement results often encompass intricate parameter interactions, and isolating each parameter's influence is often difficult.

This challenge can be mitigated with the use of deep learning or deep neural networks (DNNs), which is a potent method for uncovering complex interactions between input and output variables, and has been successfully applied in various optics research areas including image reconstruction [13, 14], optical communications [15, 16], and inverse design of optical devices [17, 18]. In addition, deep neural networks (DNNs) have been used for parameter extraction and inverse design of LDs [19, 20], in which a DNN featuring seven input design parameters and 60 output optical power values across three hidden layers was employed. The previous results demonstrated that a well-trained DNN can effectively mimic LD L-I characteristics. Furthermore, by coupling this DNN with the particle swarm optimization (PSO) method, the feasibility of inverse parameter design of LDs was demonstrated. However, in these previous research results, no specific LD structures or comparisons with measurement results were provided.

To address this gap and facilitate applications in real devices, we propose an iterative DNN structure to determine the numerical values of the Auger coefficient and the

*Corresponding author: wchoi@yonsei.ac.kr, ORCID 0000-0003-0067-4657

Color versions of one or more of the figures in this paper are available online.

pISSN: 2508-7266 / eISSN: 2508-7274

https://doi.org/10.3807/COPP.2024.8.1.80

free carrier absorption (FCA) coefficient in 850 nm GaAs/AlGaAs LDs. In Section II, as we will explain, Auger and FCA coefficients significantly affect the L-I characteristics of LDs. Traditionally, numerous repetitive comparisons between simulation and measurement results were made to determine the values of these parameters, a process that strongly depends on the researcher's expertise and requires a considerable amount of time. We propose a method that can accurately extract the Auger and FCA coefficients of the actual device using training data and the DNN. This approach is applicable not only to the LD used in this paper but also to other types of opto-electronic devices. Information about the device structure is sent to the DNN through the LD simulation using PICS3D, a commercially available software. Leveraging a dataset of 448 simulation results for DNN training and testing, a temperature-dependent model of the Auger coefficient and the value of the FCA coefficient are determined.

The remainder of this paper is structured as follows. Section II outlines the parameter extraction algorithm and the DNN structure. In Section III, we present the characteristics of fabricated LDs and validate the accuracy of extracted parameters using them. Finally, Section IV concludes the paper.

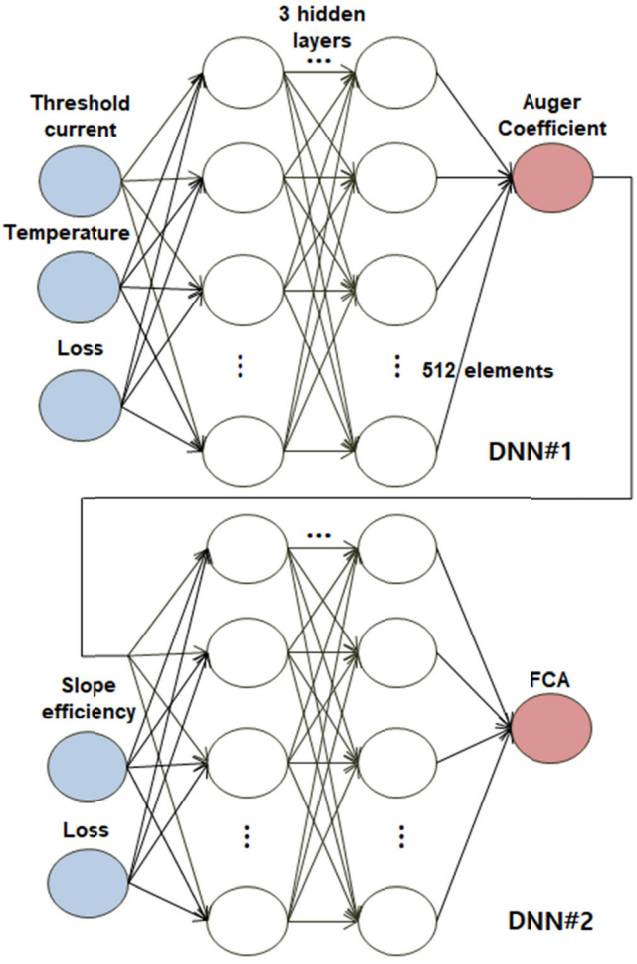

FIG. 1. Consecutive schematic structure of deep neural network (DNN).

II. ALGORITHM AND DNN STRUCTURE

The L-I characteristics of an LD typically involve two primary components of the threshold current and the slope efficiency, which are influenced by various factors, including the device's layer structure, doping density, cavity length, and material properties such as internal loss, the Auger coefficient, and the FCA coefficient. If the LD structure is known, material properties are the key factors for the L-I characteristics. Specifically, the threshold current is determined by the interplay between internal loss and the Auger coefficient [21, 22]. On the other hand, the slope efficiency is determined by internal loss, the Auger coefficient, and the FCA coefficient [22]. It is essential to accurately extract the numerical values for these parameters for analysis and device design optimization. While internal loss can be obtained experimentally, the other two parameters are often treated as fitting parameters for matching L-I characteristics measurement and simulation [22, 23].

In this study, we use two DNN structures, labeled DNN#1 and DNN#2, to accurately and efficiently extract the Auger coefficient using the threshold current, and the FCA coefficient using the slope efficiency, respectively. The consecutive DNN structures and overall workflow are shown in Figs. 1 and 2. Our approach requires two separate DNNs, each designed to extract a specific design parameter in succession. Each DNN has three input variables and one output variable, all connected through three hidden layers with 512 elements each.

The architecture of the DNNs can be adjusted based on the size of the training dataset. The DNNs use the Adam optimizer, the ReLU activation function, and the mean

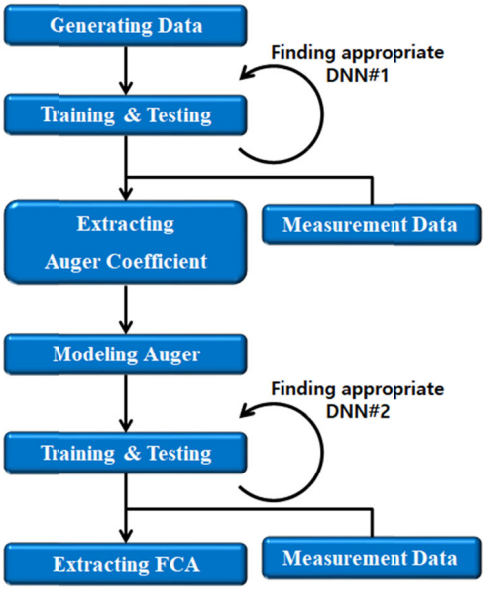

FIG. 2. Overall process of parameter extraction.

squared error (MSE) loss function, and are trained over a million epochs to achieve deep learning convergence. DNN#1 takes the threshold current, temperature, and internal loss as inputs and produces the Auger coefficient as output. DNN#2, on the other hand, takes the previously extracted Auger coefficient, the slope efficiency, and internal loss as inputs, and produces the FCA coefficient output. It is assumed that the Auger coefficient exhibits temperature dependence, while FCA is considered a constant.

Generating the necessary training data involves L-I characteristic simulations with varying values of internal loss of $[\alpha_0, \ldots, \alpha_{j-1}]$, the Auger coefficient of $[C_0, \ldots, C_{k-1}]$, the FCA coefficient of $[k_0, \ldots, k_{m-1}]$, and temperature of $[T_0, \ldots, T_{n-1}]$. To train the DNNs effectively, careful data preparation is crucial. For DNN#1, where the FCA coefficient is not a dominant factor for the threshold current, simulations are conducted with $k_0 = 0$. For DNN#2, simulations are run at a specific temperature (T_s) given the assumed absence of temperature dependence in the FCA coefficient. This strategic approach reduces the number of required simulations from $(j \times k \times m \times n)$ to $(j \times k \times n) + (j \times k \times m) - (j \times k)$. Subsequently, the generated data are split into training and testing sets.

Since the performance of the DNNs is influenced by the training data, it is essential to identify the DNN with the lowest testing loss. Thus fine-tuning is performed, with DNN#1 and DNN#2 undergoing $k - 2$ and $m - 2$ iterations of deep learning, respectively. For instance, DNN#1's testing set, comprising $j \times n$ data, is progressively trained and tested with varying Auger coefficients from C_1 to C_{k-2}. The most suitable DNN is determined by observing the minimum testing loss curve over the iterations. The final step involves using the chosen DNN with measurement data to accurately extract real device design parameters, such as Auger and FCA coefficients. For the implementation of deep learning, open-source Python and PyTorch libraries are employed.

III. PARAMETER EXTRACTION AND VALIDATION

A cross-sectional view of a sample 850 nm GaAs/AlGaAs LD is illustrated in Fig. 3. The LD comprises three 8 nm GaAs quantum wells, AlGaAs barriers, and graded refractive index separate confinement heterostructures. P-type and N-type AlGaAs layers serve as the top and bottom cladding layers. The fabricated device has a stripe width of 1 μm and a cavity length of 700 μm, and is equipped with an antireflection (AR) coating on one side (R = 0.11) and

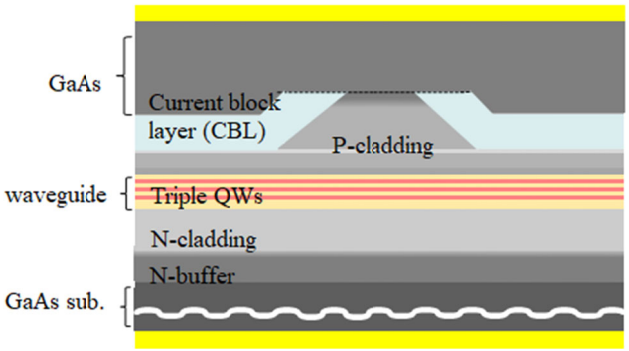

FIG. 3. Cross-section of 850 nm GaAs/AlGaAs laser diode.

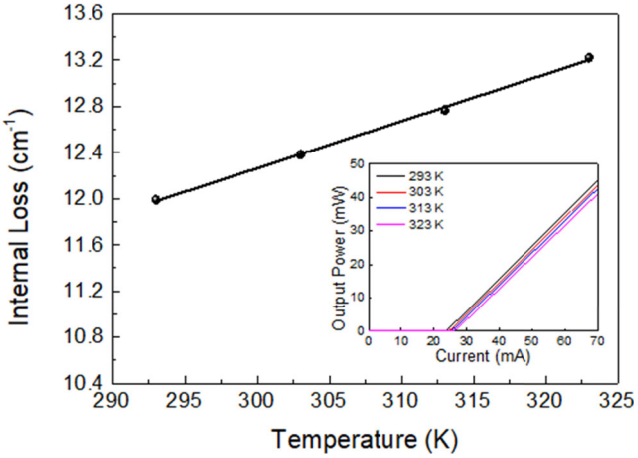

FIG. 4. Temperature dependence of internal loss of laser diode.

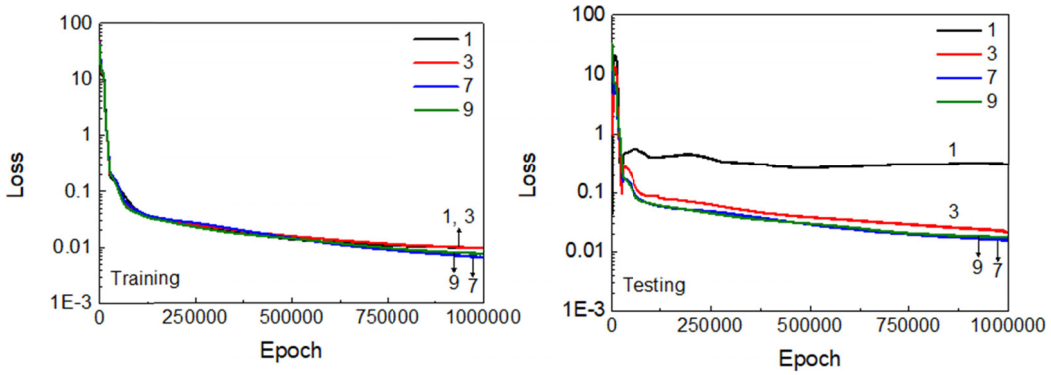

(a) (b)

FIG. 5. Loss curves of DNN#1 of (a) training and (b) testing.

high-reflection (HR) coating on the other side (R = 0.95). The temperature dependence of the LD's internal loss is measured, and the results are shown in Fig. 4. The inset shows the LD's L-I characteristics at various temperatures. Threshold currents of 23.5, 24.2, 25.4, and 26.2 mA, along with corresponding slope efficiencies of 0.983, 0.969, 0.959, and 0.943 mW/mA, are measured at 293 K, 303 K, 313 K, and 323 K, respectively. Notably, the internal loss exhibits linear dependence with temperature (T), given as $12.18 + 0.041(T - 298)$, which serves as one of the inputs for both DNNs.

A total of 448 L-I characteristic simulations are conducted, spanning different parameter values with $j = 8$, $k = 7$, $m = 5$, and $n = 4$. This simulation includes internal loss values of [1, 3, 5, 7, 9, 11, 13, 15] cm^{-1}, Auger coefficient (C) of [0, 1, 3, 5, 7, 9, 11] $\times 10^{-30}$ cm^6s^{-1} and FCA(k) of [0, 1, 2, 3, 4] $\times 10^{-18}$ cm^{-2}, all evaluated at different temperatures of [293, 303, 313, 323] K, and each range for Auger and FCA coefficient was set based on commonly known values. Figure 5 shows the training and testing loss curves of DNN#1 when the testing set's C values are [1, 3, 7, 9] $\times 10^{-30}$ cm^6s^{-1}. Notably, the absence of a curve for $C_3 = 5 \times 10^{-30}$ cm^6s^{-1} is due to underfitting. While the training loss curves suggest well-trained DNNs for all cases, Fig. 5(b) highlights that the testing set with $C_1 = 10^{-30}$ cm^6s^{-1} is unsuitable for DNN#1 because of overfitting. Consequently, the appropriate DNN#1 is determined to be the one aligned with the testing set of $C_4 = 7 \times 10^{-30}$ cm^6s^{-1}, exhibiting the minimum loss, and each training and testing loss value is 6.4 and 15.7 $\times 10^{-3}$ at an epoch of 1 million.

Leveraging this DNN#1, Auger coefficients of the LD are extracted at varying temperatures, as depicted in Fig. 6. Using a well-established model equation [24] given by $C = C_o \times \exp(E_a/k_{\text{Boltzmann}}T)$, where E_a is the activation energy and $k_{\text{Boltzmann}}$ is the Boltzmann constant, extracted values of C_o of 3.95×10^{-27} cm^6s^{-1} and E_a of 167.5 meV are obtained. The corresponding modeling curve is presented in Fig. 6, and this extracted Auger model automatically becomes an input for DNN#2.

Figure 7 shows the training and the testing curves of DNN#2 at $T_1 = 303$ K when the testing set's k values are [1, 2, 3] $\times 10^{-18}$ cm^{-2}. The absence of a curve for $k_3 = 3 \times 10^{-18}$ cm^{-2} is due to underfitting. Notably, the suitable DNN#2 is found for the testing set aligned with $k_2 = 2 \times 10^{-18}$ cm^{-2}, as shown in Fig. 7(b), and each value of training and testing loss is 0.8 and 14.5×10^{-3} at an epoch of 1 million. Consequently, the extracted FCA coefficient is determined to be 1.01×10^{-18} cm^{-2}.

Finally, a verification process is conducted to validate the accuracy of the extracted values. The L-I characteristics are recalculated using the extracted parameters across various temperatures. The simulation results and the measured data are compared in Fig. 8 at various temperatures, showing a close alignment between the two.

IV. CONCLUSION

The Auger and FCA coefficients of the GaAs/AlGaAs-based 850 nm LD, the focal device in this investigation, were effectively obtained with a methodological approach designed to reduce dependence on the researcher's expertise and enhance accuracy. Conclusively, the study has showcased the successful extraction of crucial parameters

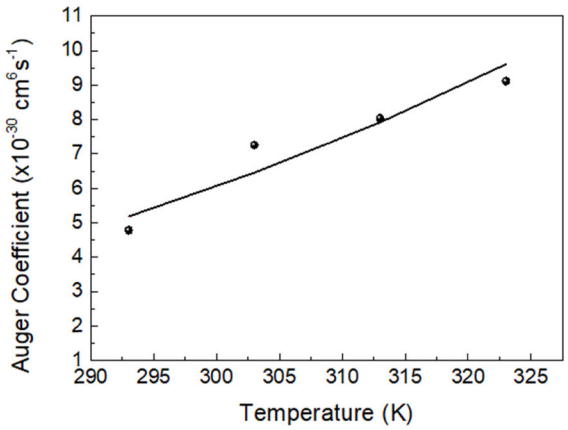

FIG. 6. Extracted values and curve of Auger coefficient.

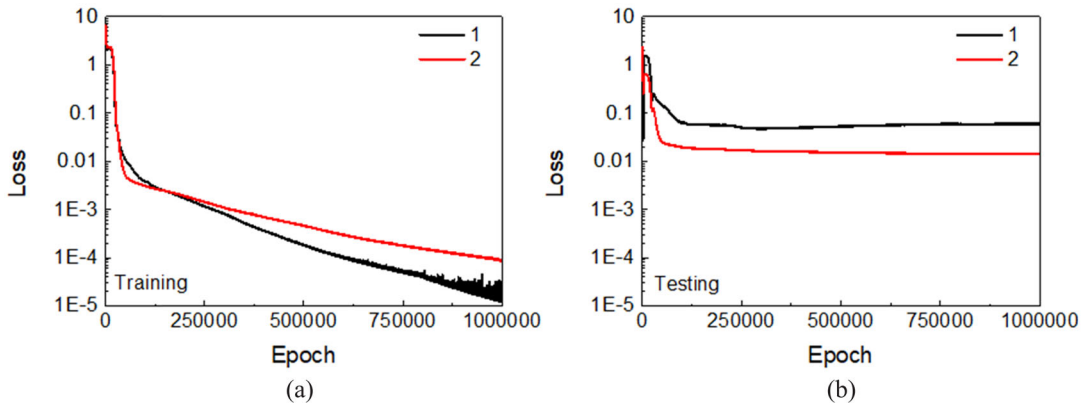

FIG. 7. Loss curves of DNN#2 of (a) training and (b) testing.

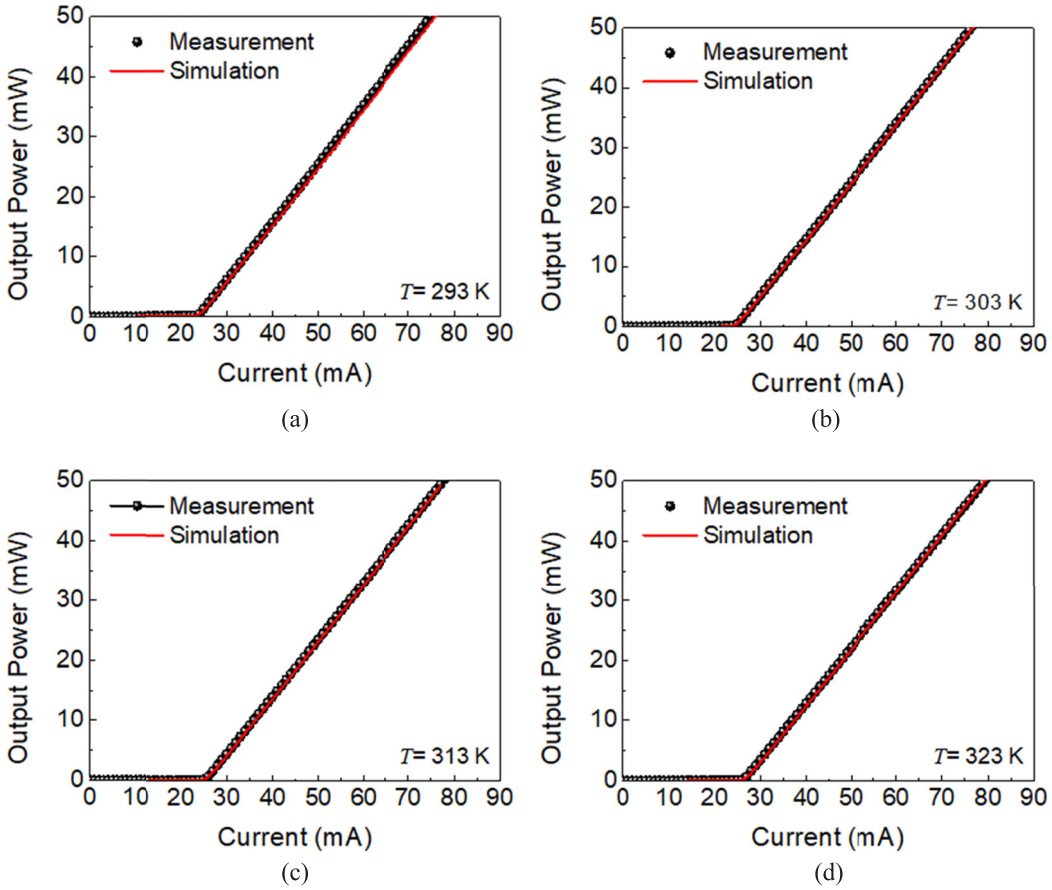

FIG. 8. L-I characteristics of simulation and measurement at (a) 293 K, (b) 303 K, (c) 313 K, and (d) 323 K using extracted parameters.

from the 850 nm GaAs/AlGaAs LD using a direct and sequential DNN system. This extraction process is carried out sequentially to ensure each parameter's uniqueness and mitigate the presence of multiple feasible values. The reliability of the extracted parameter values was verified by comparing the measured L-I characteristics with simulation results using the extracted parameters. This research is expected to apply to other LD components and aid in the design optimization and performance enhancement of the components.

FUNDING

The authors received no financial support for the research, authorship, and publication of this article.

DISCLOSURES

The authors declare that they have no known competing financial interests or personal relationships that could have appeared to influence the work reported in this paper.

DATA AVAILABILITY

Data that support the findings of this study are available from the corresponding author upon reasonable request.

REFERENCES

1. P. Crump, G. Erbert, H. Wenzel, C. Frevert, C. M. Schultz, K.-H. Hasler, R. Staske, B. Sumpf, A. Maaßdorf, F. Bugge, S. Knigge, and G. Tränkle, "Efficient high-power laser diodes," IEEE J. Sel. Top. Quantum Electron. **19**, 1501211–1501211 (2013).
2. D. Xu, Z. Guo, T. Zhang, K. Song, W. Guo, B. Wang, R. Xu, and X. Chen, "600 W high brightness diode laser pumping source," Proc. SPIE **10086**, 1008603 (2017).
3. M. Kelemen, J. Gilly, P. Friedmann, S. Hilzensauer, L. Ogrodowski, H. Kissel, and J. Biesenbach, "Diode lasers optimized in brightness for fiber laser pumping," Proc. SPIE **10514**, 10514F (2018).
4. T. H. Kim, N.-J. Kim, and J.-I. Youn, "Evaluation of wavelength-dependent hair growth effects on low-level laser therapy: An experimental animal study," Lasers Med. Sci. **30**, 1703–1709 (2015).
5. V. Knappe, F. Frank, and E. Rohde, "Principles of lasers and

biophotonic effects," Photomed. Laser Surg. **22**, 411–417 (2004).
6. H. M. Oubei, C. Li, K.-H. Park, T. K. Ng, M.-S. Alouini, and B. S. Ooi, "2.3 Gbit/s underwater wireless optical communications using directly modulated 520 nm laser diode," Opt. Express **23**, 20743–20748 (2015).
7. H. Kawaguchi, "Bistable laser diodes and their application: State of the art," IEEE J. Sel. Top. Quantum Electron. **3**, 1254–1270 (1997).
8. T. Zheng, G. Shen, Z. Li, L. Yang, H. Zhang, E. Wu, and G. Wu, "Frequency-multiplexing photon-counting multi-beam LiDAR," Photonics Res. **7**, 1381–1385 (2019).
9. I. Vornicu, J. M. López-Martínez, F. N. Bandi, R. C. Galán, and Á. Rodríguez-Vázquez, "Design of high-efficiency SPADs for LiDAR applications in 110 nm CIS technology," IEEE Sens. J. **21**, 4776–4785 (2021).
10. J.-E Joo, M.-J. Lee, and S. M. Park, "A CMOS fully differential optoelectronic receiver for short-range LiDAR sensors," IEEE Sens. J. **23**, 4930–4939 (2023).
11. S. I. Bae, S. Lee, J.-M. Kwon, H.-K. Kim, K.-W. Jang, D. Lee, and K.-H. Jeong, "Machine-learned light-field camera that reads facial expression from high-contrast and illumination invariant 3D facial image," Adv. Intell. Syst. **4**, 2100182 (2021).
12. J. Cheng, X. Sun, S. Zhou, X. Pu, N. Xu, Y. Xu, and W. Liu, "Ultra-compact structured light projector with all-dielectric metalenses for 3D sensing," AIP Adv. **9**, 105016 (2019).
13. Y. Rivenson, Y. Zhang, H. Günaydın, D. Teng, and A. Ozcan, "Phase recovery and holographic image reconstruction using deep learning in neural networks," Light Sci. Appl. **7**, 17141 (2017).
14. B. Yao, W. Li, W. Pan, Z. Yang, D. Chen, J. Li, and J. Qu, "Image reconstruction with a deep convolutional neural network in high-density super-resolution microscopy," Opt. Express **28**, 15432–15446 (2020).
15. T. Koike-Akino, Y. Wang, D. S. Millar, K. Kojima, and K. Parsons, "Neural turbo equalization: Deep learning for fiber-optic nonlinearity compensation," J. Light. Technol. **38**, 3059–3066 (2020).
16. B. Rahmani, D. Loterie, G. Konstantinou, D. Psaltis, and C. Moser, "Multimode optical fiber transmission with a deep learning network," Light Sci. Appl. **7**, 69 (2018).
17. X. Han, Z. Fan, Z. Liu, C. Li, and L. J. Guo, "Inverse design of metasurface optical filters using deep neural network with high degrees of freedom," InfoMat **3**, 432–442 (2020).
18. T. Zhao, W. Ji, P. Liu, F. Gao, C. Li, Y. Wang, and W. Huang, "Highly efficient inverse design of semiconductor optical amplifiers based on neural network improved particle swarm optimization algorithm," IEEE Photonics J. **15**, 8500409 (2023).
19. Z. Ma, P. Feng, and Y. Li, "Inverse design of semiconductor laser parameters based on deep learning and particle swarm optimization method," Proc. SPIE **11209**, 112092X (2019).
20. Z. Ma and Y. Li, "Parameter extraction and inverse design of semiconductor lasers based on the deep learning and particle swarm optimization method," Opt. Express **28**, 21971–21981 (2020).
21. J. R. Meyer, C. L. Canedy, M. Kim, C. S. Kim, C. D. Merritt, W. W. Bewley, and I. Vurgaftman, "Comparison of Auger coefficients in type I and type II quantum well midwave infrared lasers," IEEE J. Quantum Electron. **57**, 2500110 (2021).
22. J. Piprek, P. Abraham, and J. E. Bowers, "Self-consistent analysis of high-temperature effects on strained-layer multiquantum-well InGaAsP-InP lasers," IEEE J. Quantum Electron. **36**, 366–374 (2000).
23. J. Piprek, P. Abraham, and J. E. Bowers, "Cavity length effects on internal loss and quantum efficiency of multiquantum-well lasers," IEEE J. Sel. Top. Quantum Electron **5**, 643–647 (1999).
24. J. Piprek, J. K. White, and A. J. SpringThorpe, "What limits the maximum output power of long-wavelength AlGaInAs/InP laser diodes?," IEEE J. Quantum Electron. **38**, 1253–1259 (2002).